Electronic Supplementary Material (ESI) for Journal of Materials Chemistry C.

SUPPLEMENTARY INFORMATION

Band Gap Tuning Through Cation and Halide Alloying in Mechanochemical Synthesized $Cs_3(Sb_{1-x}Bi_x)_2Br_9$ and $Cs_3Sb_2(I_{1-x}Br_x)_9$ Solid Solutions

*Giulia Giovilli,[a] Benedetta Albini,[b] Virginia Grisci,[c] Sara Bonomi,[a] Marco Moroni,[a] Edoardo Mosconi,[d] Waldemar Kaiser, [d] Filippo De Angelis, [c,d,e,f] Pietro Galinetto,[b] Lorenzo Malavasi[a,]**

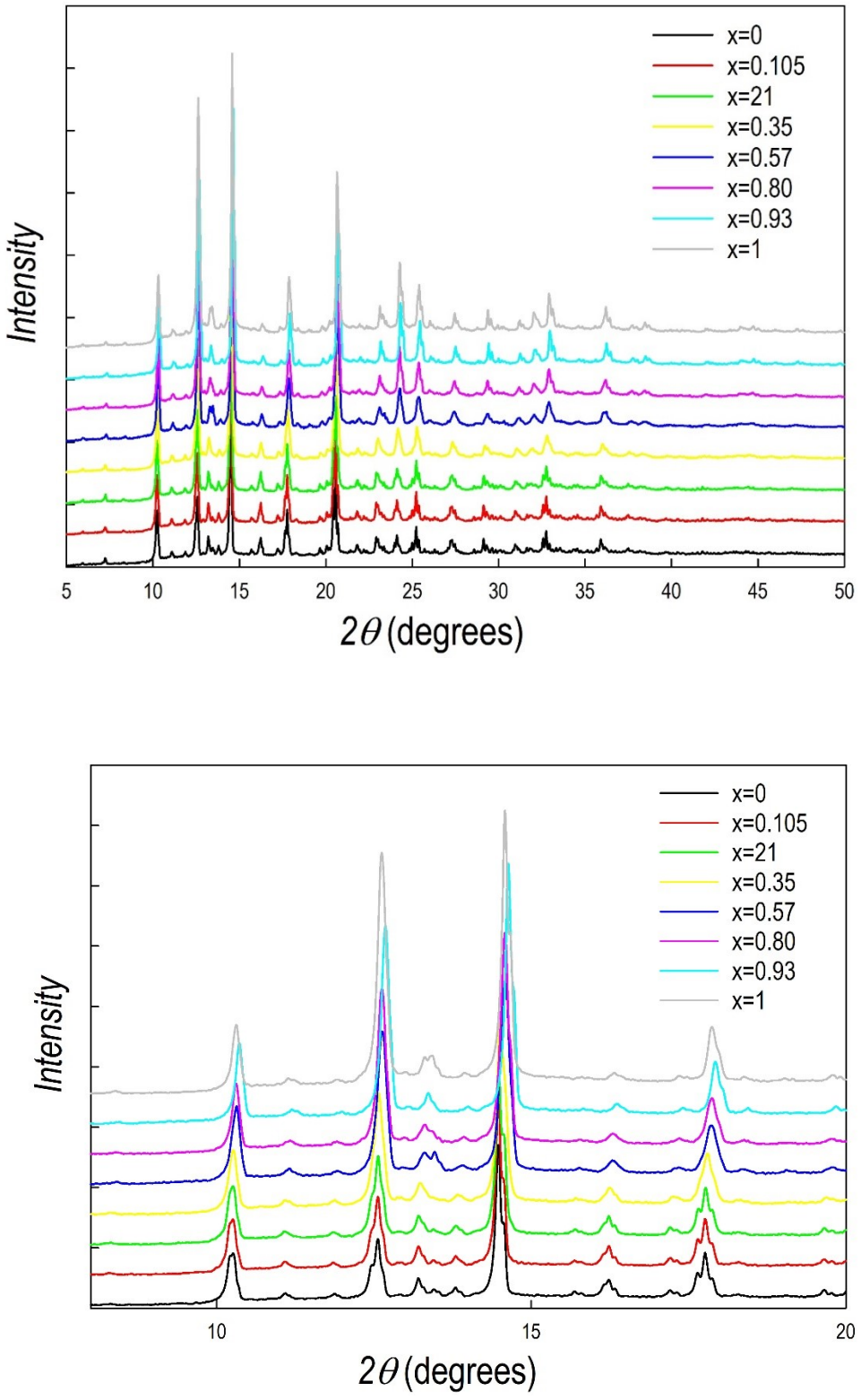

Figure S1. a) XRD pattern of a $Cs_3(Sb_{1-x}Bi_x)_2Br_9$ solid solution as a function of x measured with Mo-K radiation in transmission mode; b) same patterns in a reduced 2-theta range.

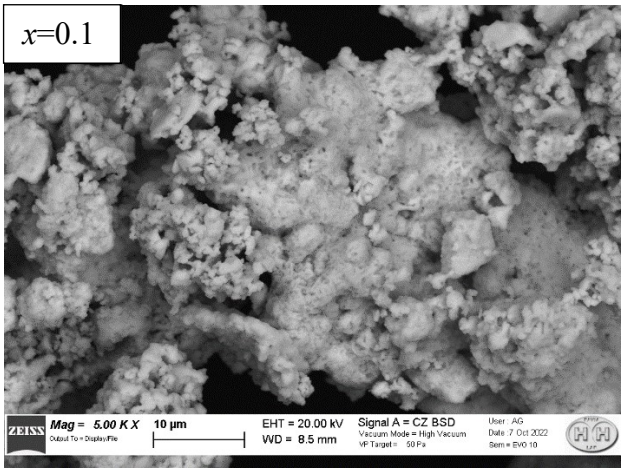
x=0.1
ZEISS Mag = 5.00 K X 10 µm EHT = 20.00 kV WD = 8.5 mm Signal A = CZ BSD Vacuum Mode = High Vacuum VP Target = 50 Pa User : AG Date :7 Oct 2022 Sem = EVO 10

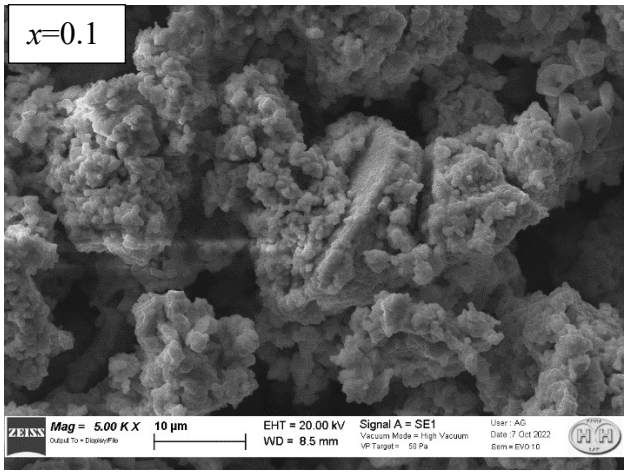
x=0.1
ZEISS Mag = 5.00 K X 10 µm EHT = 20.00 kV WD = 8.5 mm Signal A = SE1 Vacuum Mode = High Vacuum VP Target = 50 Pa User : AG Date :7 Oct 2022 Sem = EVO 10

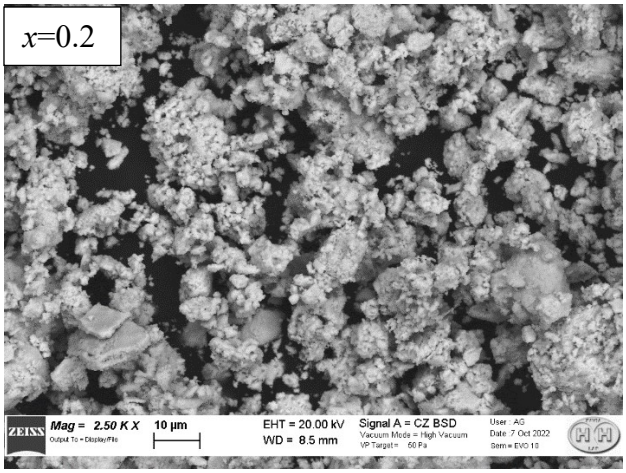
x=0.2
ZEISS Mag = 2.50 K X 10 µm EHT = 20.00 kV WD = 8.5 mm Signal A = CZ BSD Vacuum Mode = High Vacuum VP Target = 50 Pa User : AG Date :7 Oct 2022 Sem = EVO 10

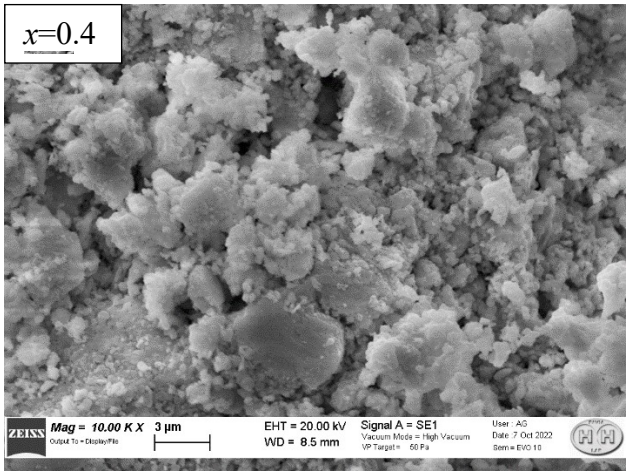
x=0.4
ZEISS Mag = 10.00 K X 3 µm EHT = 20.00 kV WD = 8.5 mm Signal A = SE1 Vacuum Mode = High Vacuum VP Target = 50 Pa User : AG Date :7 Oct 2022 Sem = EVO 10

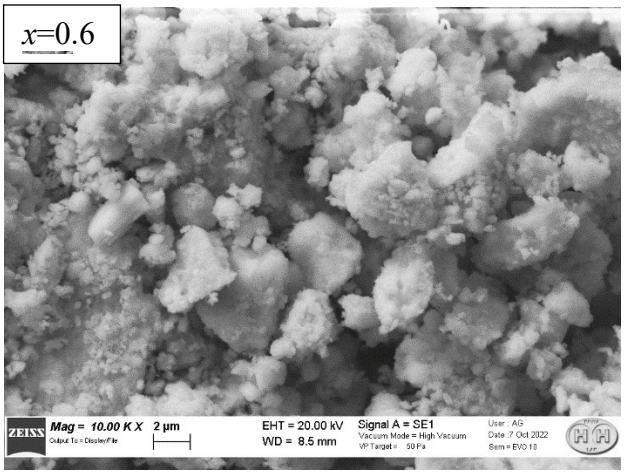
x=0.6
ZEISS Mag = 10.00 K X 2 µm EHT = 20.00 kV WD = 8.5 mm Signal A = SE1 Vacuum Mode = High Vacuum VP Target = 50 Pa User : AG Date :7 Oct 2022 Sem = EVO 10

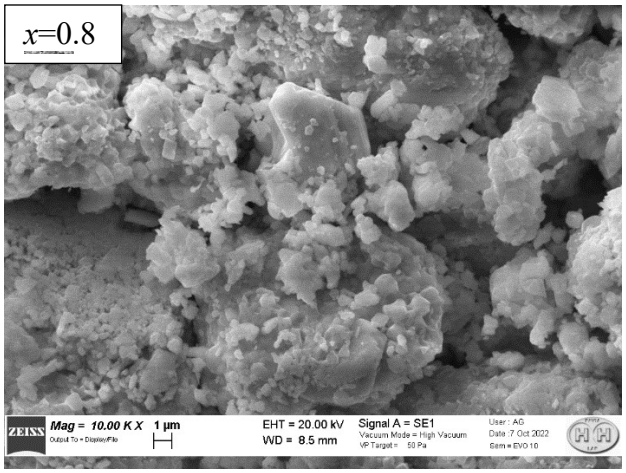
x=0.8
ZEISS Mag = 10.00 K X 1 µm EHT = 20.00 kV WD = 8.5 mm Signal A = SE1 Vacuum Mode = High Vacuum VP Target = 50 Pa User : AG Date :7 Oct 2022 Sem = EVO 10

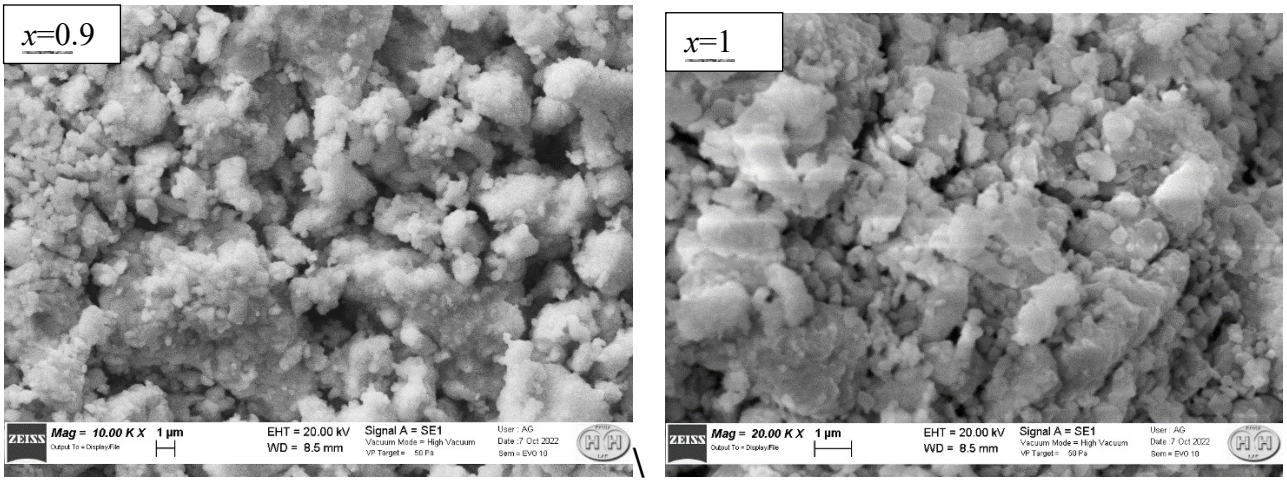

Figure S2. SEM images for the samples of the $Cs_3(Sb_{1-x}Bi_x)_2Br_9$ system.

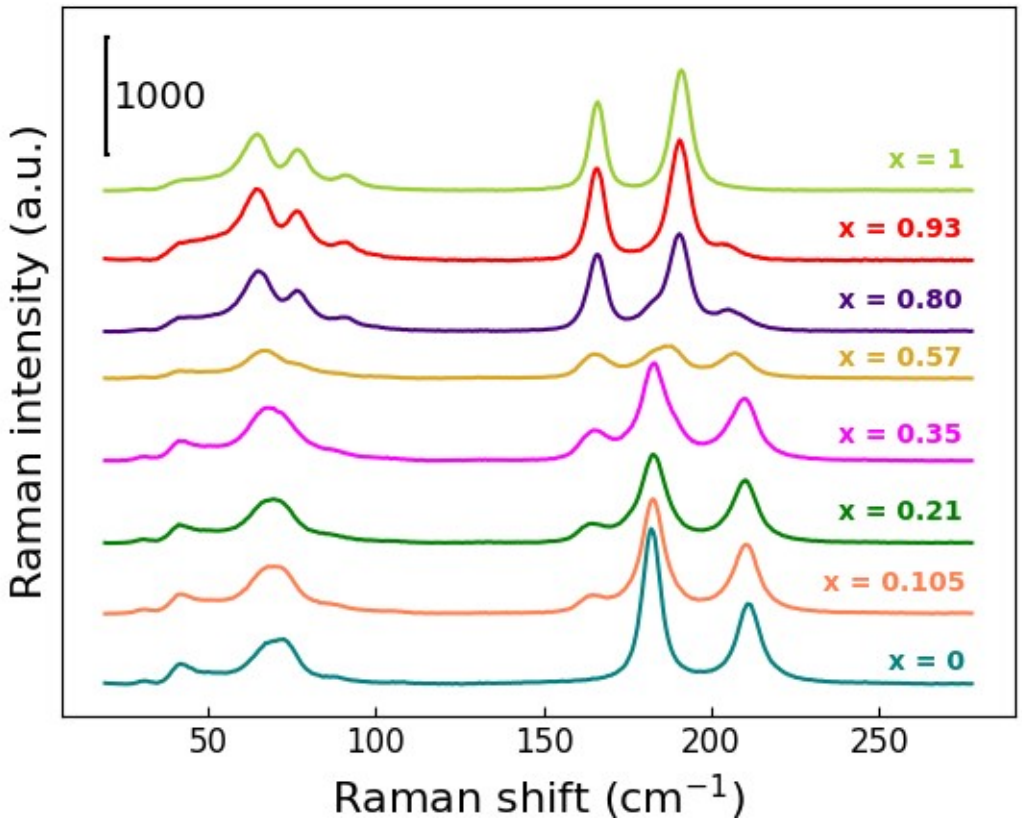

Figure S3. RT Raman spectra of the $Cs_3(Sb_{1-x}Bi_x)_2Br_9$ samples.

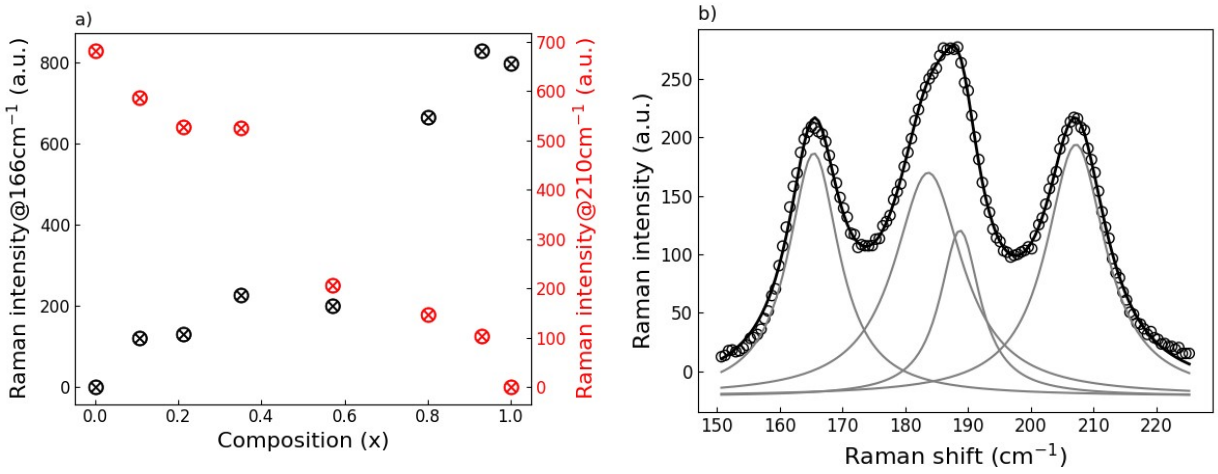

Figure S4. a) Raman intensity of the mode at 166 and 210 cm^{-1} proper of $Cs_3Bi_2Br_9$ and $Cs_3Sb_2Br_9$ structures, respectively. b) Best fitting procedure performed with four Lorentzian functions (grey lines) on the Raman spectrum (scattered one) of $x = 0.57$ sample.

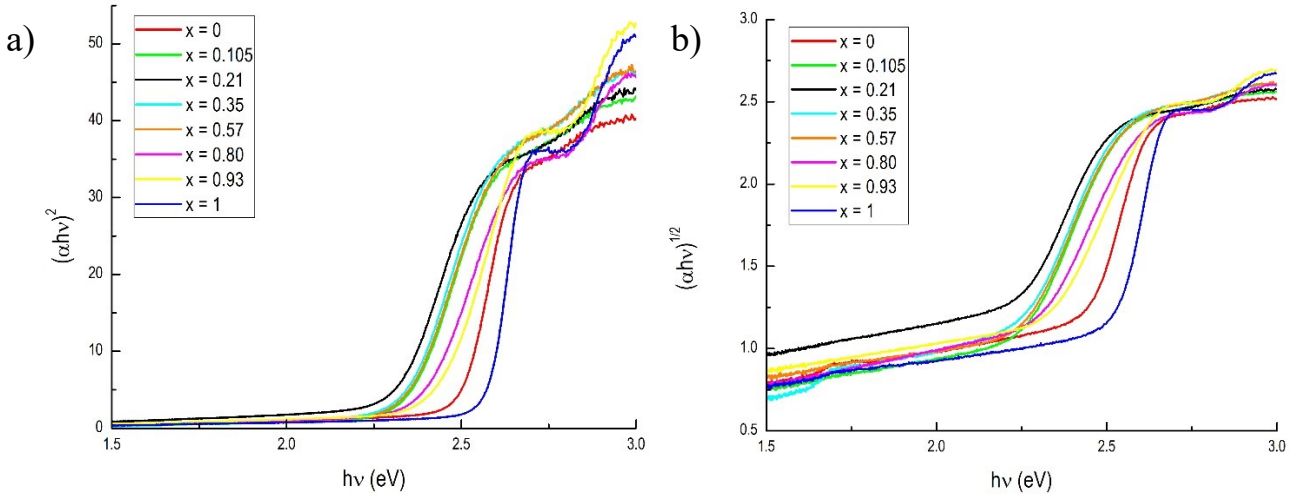

Figure S5. Tauc plots for (a) direct and (b) indirect transition of the $Cs_3(Sb_{1-x}Bi_x)_2Br_9$ solid solution.

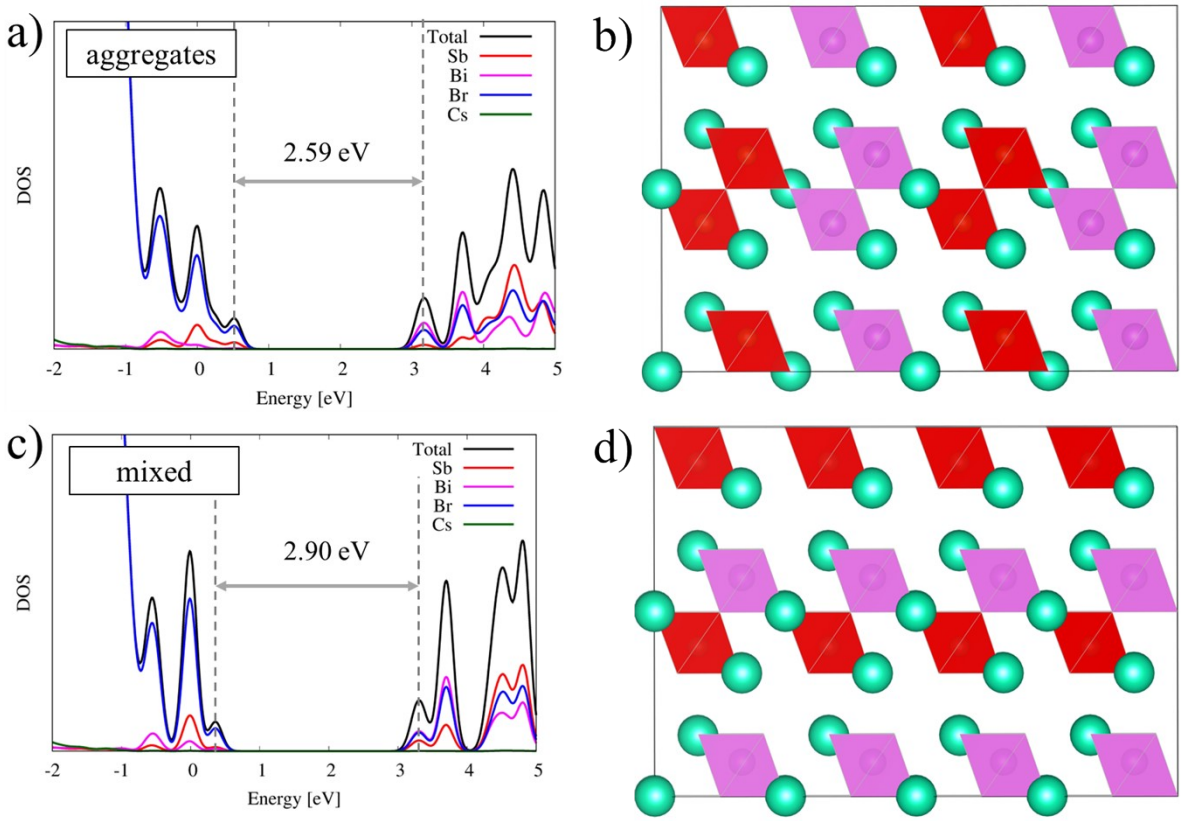

Figure S6. (a,b) Density of states (DOS) and structural representation of the $Cs_3SbBiBr_9$ system with local aggregation of Sb- and Bi-centered octahedra. (c,d) Density of states and structural representation of the $Cs_3SbBiBr_9$ with fully dispersed Sb- and Bi-centered octahedra. DFT-HSE06+SOC band gap are shown explicitly in the DOS.

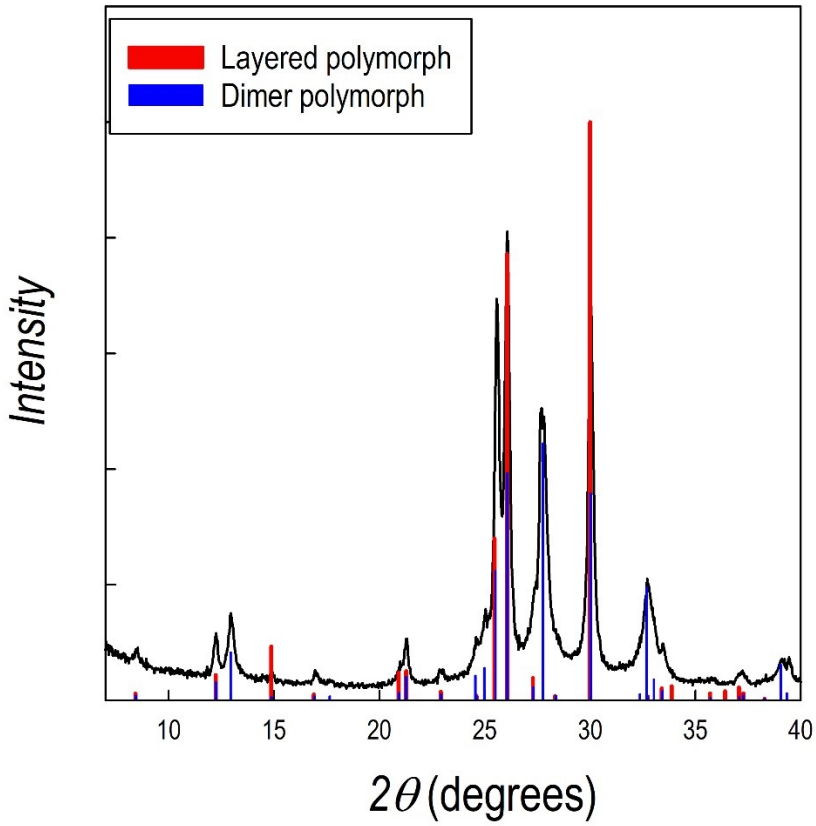

Figure S7. XRD pattern of $Cs_3Sb_2I_9$ obtained at 400 rpm with 6 milling cycles. Blue and red vertical bars refer to the calculated pattern for the dimer and layered polymorphs, respectively.

Experimental

Synthesis of $Cs_3(Sb_{1-x}Bi_x)_2Br_9$ *and* $Cs_3Sb_2(Br_{1-x}I_x)_9$

The perovskites were prepared by mechanochemical solid-state synthesis: powder $CsBr$ (99%, Alfa-Aesar), $SbBr_3$(99.5%, Alfa-Aesar) and $BiBr_3$ (99%, Alfa-Aesar) were added in stoichiometric quantities $(x = 0, 0.2, 0.4, 0.8, 1.2, 1.6, 1.8, 2)$ inside a tungsten carbide (WC) planetary grinding bowl with WC grinding balls $(d_{ball} = 5\ mm)$ in a ratio of 1 g of desired product to 10 g of balls. The mechanochemical synthesis was carried out in a Fritsch Planetary Micro Mill PULVERISETTE 7 employing 6 cycles (20 minutes of grinding plus a 10-minute pause) at 400 rpm. The same procedure was applied for the synthesis of the $Cs_3Sb_2(Br_{1-x}I_x)_9$ solid solution employing, in this case $CsBr$ (99%, Alfa-Aesar), CsI(99.9%, Sigma-Aldrich), $SbBr_3$(99.5%, Alfa-Aesar) and SbI_3 (98%, Sigma-Aldrich). The powders were added in stoichiometric quantities $(x = 0, 2.5, 4.5, 6.5, 9)$ inside a tungsten carbide (WC) planetary grinding bowl as in the previous synthesis and the grinding was applied for 10 cycles (20 minutes of grinding plus a 10-minute pause) at 600 rpm

X-ray Diffraction. The crystal structure of the samples has been characterized by room temperature Cu-K and Mo-K radiation XRD acquired with Bruker D8 Advances diffractometers. Diffraction experiments were carried out in flat-plate mode by using null-background sample holders.

UV-Vis spectroscopy. DRS spectra were acquired in the wavelength range 300- 800 nm directly on the powders by using a Jasco V-750 spectrophotometer, equipped with an integrating sphere (Jasco ISV-922). The Tauc method was employed to determine the direct and indirect band gap values. The method is based on the following equation: $(\alpha \times h\nu)^{\frac{1}{\gamma}} = B(h\nu - E_g)$ where h is the Planck constant, ν is the photon's frequency, E_g is the band gap energy, and B is a constant. The γ factor depends on the nature of the electron transition and is equal to 1/2 or 2 for the direct and indirect transition band gaps, respectively.

Scanning Electron Microscopy. SEM micrographs of the samples were collected by a Zeiss EVO MA10 (Carl Zeiss, Oberkochen, Germany) microscope, equipped with an energy dispersive detector for the EDS analysis, on gold-sputtered samples (20 kV, secondary electron images, working distance 8.5 mm).

Raman spectroscopy. Micro-Raman measurements were carried out at room temperature by means of the automated and integrated confocal XploRA Plus spectrometer, HORIBA Scientific, equipped with an Olympus microscope BX43. Three different laser sources are available: 532 nm, 100 mW, 638 nm, 90 mW, and 785 nm, 100 mW. Neutral filters with different optical density allow to set the incident laser power. The spectrometer is equipped with a motorized xy stage on which the investigated samples are positioned. Spectral resolution is about 1 cm^{-1}. An Open Electrode CCD camera, with a multistage Peltier air-cooling system, is used as detector.

The measurements were performed at room temperature with the 638 nm laser source, using a 50x magnification objective with a spot sizes of 4 μm^2 , a neutral filter such that the 0.1% of the incoming laser power arrived to the sample. Since the Raman activity of these samples is extremely intense only 2 s of integration time were needed, together with 10 accumulations. All the reported spectra are the result of an average of spectra collected at different points in each sample.

Theoretical Details

All calculations have been carried out using Quantum Espresso program package. [1] As a first approach we start from the experimental cell parameters of pure Sb and Bi material and we carried out a variable cell relaxation at PBE [2] level with 50/400 Ry as planewave and density cutoff along with standard scalar relativistic ultrasoft pseudo potentials. The angles of the cell were kept fixed to the experimental values. See optimized cell parameters in Table S1. A k-point mesh grid of 2x2x2 was used. To simulate the mixed Sb/Bi material we move to simulate a 2x2x1 supercell to allow us to modify the Sb and Bi distribution in the crystal structure. In all geometry optimization D3 dispersion interactions[3] were included. The electronic properties (band gap and DOS) were simulated on the optimized geometries as a single point at HSE06 [4] level including spin orbit coupling (SOC) with a 40 Ry as a plain wave cutoff. For the hybrid functional calculation norm-conserving pseudo potential have been used with 9 and 7 electrons for Cs and Br, while for Bi and Sb were used pseudo potential with 23 electrons. An increased fraction of exact exchange α=0.43,4 SOC included, provides an accurate estimate of the electronic properties of perovskites in agreement with state of the art GW calculations and experiments.[5-6] A survey of the theoretical results and method validation are reported in Table S2.

As we can see, the calculated band gap on the 1x1x1 supercell with a k-point grid of 2x2x2 are essentially the same calculated on the 2x2x1 supercell with a k point grid of 1x1x2. To further check the convergence of the model we also tested a k-point grid of 2x2x2 on the o-$Cs_3SbBiBr_9$ supercell obtaining similar results in term of band gap.

Table S1. Variable cell optimized lattice vectors in Å. The values of the 2x2x1 are normalized to the 1x1x1 supercell.

Supercell		1x1x1			2x2x1		
k-point mesh		2 2 2			2 2 2		
$Cs_3Sb_2Br_9$	a	8.00	0.00	0.00	-	-	-
	b	-3.96	6.94	0.00	-	-	-
	c	0.00	0.00	9.81	-	-	-
d-$Cs_3SbBiBr_9$	a	8.04	0.00	0.00	8.01	0.00	0.00
	b	-3.96	6.98	0.00	-3.96	6.95	0.00
	c	0.00	0.00	9.87	0.00	0.00	9.89
o-$Cs_3SbBiBr_9$	A	-	-	-	8.01	0.00	0.00
	b	-	-	-	-3.96	6.95	0.00
	c	-	-	-	0.00	0.00	9.89
$Cs_3Bi_2Br_9$	a	8.06	0.00	0.00	-	-	-
	b	-3.99	6.99	0.00	-	-	-
	c	0.00	0.00	9.93	-	-	-

Table S2. Calculated direct and indirect band gap (eV) at different level of model.

Supercell	1x1x1		2x2x1			
k-point mesh	2 2 2		1 1 2		2 2 2	
HSE06-SOC - HF=43%	Gap Ind.	Gap Dir.	Gap Ind.	Gap Dir.	Gap Ind.	Gap Dir.
$Cs_3Sb_2Br_9$	2.90	2.94	2.91	2.96	-	-
Mixed $Cs_3SbBiBr_9$	2.88	2.98	2.90	3.00	-	-
Aggregated $Cs_3SbBiBr_9$	-	-	2.59	2.71	2.57	2.79
$Cs_3Bi_2Br_9$	2.94	3.07	2.97	3.10	-	-

References:

1. Giannozzi, P.; Baroni, S.; Bonini, N.; Calandra, M.; Car, R.; Cavazzoni, C.; Ceresoli, D.; Chiarotti, G. L.; Cococcioni, M.; Dabo, I.; Corso, A. D.; de Gironcoli, S.; Fabris, S.; Frates, G.; Gebauer, R.; Gerstmann, U.; Gougoussis, C.; Kokalj, A.; Lazzeri, M.; Martin-Samos, L.; Marzari, N.; Mauri, F.; Mazzarello, R.; Paolini, S.; Pasquarello, A.; Paulatto, L.; Sbraccia, C.; Scandolo, S.; Sclauzero, G.; Seitsonen, A. P.; Smogunov, A.; Umari, P.; Wentzcovitch, R. M. QUANTUM ESPRESSO: A Modular and Open-Source Software Project for Quantum Simulations of Materials *J. Phys.: Condens. Matter* **2009,** *21*, 395502.

2. Perdew, J. P.; Burke, K.; Ernzerhof, M. Generalized Gradient Approximation Made Simple *Phys. Rev. Lett.* **1996,** *77*, 3865-3868.

3. Smith, D. G. A.; Burns, L. A.; Patkowski, K.; Sherrill, C. D. Revised Damping Parameters for the D3 Dispersion Correction to Density Functional Theory *J. Phys. Chem. Lett.* **2016,** *7*, 2197-2203.

4. Heyd, J.; Scuseria, G. E.; Ernzerhof, M. Hybrid Functionals Based on a Screened Coulomb Potential *J. Chem. Phys.* **2003,** *118*, 8207-8215.

5. Umari, P.; Mosconi, E.; De Angelis, F. Relativistic GW Calculations on $CH_3NH_3PbI_3$ and $CH_3NH_3SnI_3$ Perovskites for Solar Cell Applications *Sci. Rep.* **2014,** *4*, 4467.

6. Mosconi, E.; Umari, P.; De Angelis, F. Electronic and optical properties of $MAPbX_3$ perovskites (X = I, Br, Cl): a unified DFT and GW theoretical analysis *Phys. Chem. Chem. Phys.* **2016,** *18*, 27158-27164.